ACS APPLIED MATERIALS & INTERFACES

Research Article

Cite This: ACS Appl. Mater. Interfaces 2019, 11, 30228−30233

www.acsami.org

Self-Assembly Three-Dimensional Porous Carbon Networks for Efficient Dielectric Attenuation

Xiaohui Liang,[†,‡] Bin Quan,[†] Zengming Man,[†] Bingchen Cao,[‡,§] Nan Li,[‡,∥] Chenhao Wang,[‡,∥] Guangbin Ji,*[,†] and Ting Yu*[,‡]

[†]College of Materials Science and Technology, Nanjing University of Aeronautics and Astronautics, No. 29 Yudao Street, Nanjing 210016, P. R. China

[‡]Division of Physics and Applied Physics, School of Physical and Mathematical Sciences, Nanyang Technological University, 637371, Singapore

[§]Shaanxi Institute of Flexible Electronics (SIFE), Northwestern Polytechnical University (NPU), Xi'an 710129, China

[∥]State Key Laboratory of Solidification Processing, Center for Nano Energy Materials, School of Materials Science and Engineering, Northwestern Polytechnical University and Shaanxi Joint Laboratory of Graphene (NPU), Xi'an 710072, China

Supporting Information

ABSTRACT: Zeolitic imidazolate framework (ZIF-8)-derived ZnO/nanoporous carbon (NPC) aligned in a three-dimensional porous carbon network (3DPCN) is designed to form a multiporous network nanostructure to absorb electromagnetic waves. The porous 3DPCN structure acts as the electronic pathway and the nucleation locus for ZIF-8 particles. Meanwhile, the conductive networks could also provide more routes for electron transfer. With good impedance matching and attenuation characteristics, ZnO@NPC/3DPCN shows enhanced microwave response where the minimum reflection loss of −35.7 dB can be achieved with a 10 wt % filler. Our study not only exploits the new system of lightweight absorbers but also further reveals the changing of electromagnetic parameters and absorbing properties by heat treatment, which may lead to a new way to design novel lighter multiporous network nanostructures.

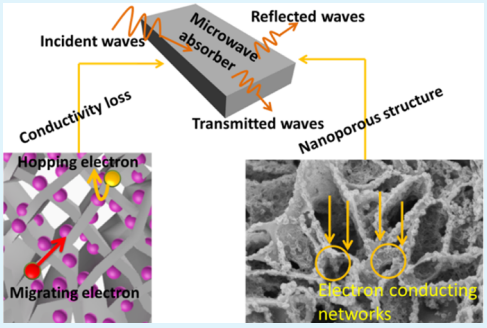

KEYWORDS: *three dimensional, metal−organic frameworks, multi-porous network, electron conductivity, impedance matching*

INTRODUCTION

Three-dimensional porous carbon networks (3DPCNs) have been exploited comprehensively, owing to the merits of interconnected porous networks, high electrical conductivity, and controllable pore-size distribution.[1] Currently, three-dimensional carbon networks are used to fabricate composites, which act as conventional substrates or backbones, and have gained great achievements in energy storage and conversion.[2,3] However, poor impedance matching caused by the single attenuation mechanism and high conductivity has hindered their further applications, when the pure three-dimensional carbon networks are introduced as microwave absorbing materials.[4,5] Based on our previous study,[6] the introduction of metal−organic framework (MOF) materials on 3DPCNs may sufficiently improve the performance of microwave absorbing.

MOFs have attracted extensive attention because of their various structures, tunable porosity, outstanding physical/chemical performance, and larger specific surface area.[7,8] Acting as sacrificial templates for synthesizing metal or metal oxides by removing the organic linkers via calcination[9−12] is a typical way to utilize MOFs as microwave absorbers. Professor Yamauchi proposed the direct carbonization method for MOF-carbons, which usually keep the same morphology as the precursor MOFs.[13] Based on this method, various kinds of metal/metal oxide structures have been fabricated, such as yolk−shell NiO/Ni/GN@Air@NiO/Ni/GN,[9] Fe−Co/nanoporous carbon (NPC),[10] Fe_3O_4 nanospheres,[11] Co_3O_4 nanoparticles on the surface of carbon fibers,[12] Zn/Co porous amorphous carbon,[14] carbonaceous ZnO/RGO,[15] Co-MOF-derived Co_3O_4,[16] Co/C@V_2O_3 hollow spheres,[17] and Fe/polyaniline.[18] In addition, good stability of the MOFs is another merit applied in microwave absorption.[19] Based on the previous studies, the zeolitic imidazolate framework (ZIF-8) nanoparticles and their generating NPC possess better stability applied in many areas,[20−24] such as ZIF-8-derived nanoporous carbon used as organic electrolyte,[21] energy storage,[22] supercapacitor devices,[23] and energy conversion devices.[24] However, developing MOF-aligned three-dimensional carbon network composites as a microwave absorption material is still a challenge because of the poor contact and nonuniform dispersion within the two constituents.

Received: May 14, 2019
Accepted: July 30, 2019
Published: July 30, 2019

DOI: 10.1021/acsami.9b08365
ACS Appl. Mater. Interfaces 2019, 11, 30228−30233

In this study, ZIF-8 particles were in situ grown in 3DPCNs to form multiporous network nanostructures. In this structure, ZIF-8-derived ZnO@NPC nanoparticles via direct carbonization were uniformly anchored in the interconnected carbon network and plays a role of regulating impendence matching of hybrids. Such unique structure not only provides more contact sites for microwave but also improves the impedance matching of the composites. The obtained composite, acting as the microwave absorber, presents an outstanding performance, in which its maximum reflection loss (RL) value can reach −35.7 dB with a filler loading ratio of 10 wt %.

EXPERIMENTAL SECTION

3DPCN Synthesis. 3DPCNs were synthesized by a self-assembly method, in which glucose and sodium carbonate were used as a carbon source and template, respectively.[25] In the typical synthesis process, 20 g sodium carbonate and 1.25 g glucose were added into deionized water and stirred for 2 h. The precursor solution was then freeze-dried for 48 h, and the resulting white powders were collected and calcined at 700 °C for 2 h under an Ar atmosphere. After removing the template, 3DPCNs were obtained.

Preparation of ZnO@NPC/3DPCN. For the preparation of ZnO@NPC/3DPCN hybrids, 30 mg of 3DPCNs and 1.1 mmol $Zn(NO_3)_2{\cdot}6H_2O$ were dissolved in 25 mL absolute methanol and stirred for 5 min. Meanwhile, 217 mg 2-methylimidazole (2-MeIm) was dissolved in 25 mL absolute methanol, and then added into the above suspension. The mixture was maintained for 24 h without stirring. Finally, ZIF-8/3DPCN hybrids were washed with methanol, and then dried at 60 °C for 12 h. Then the samples were calcined at 500 °C under an Ar atmosphere in a tubular furnace, and the ZnO@NPC/3DPCN powders were obtained. According to the calcination reaction temperature of 500, 600, and 700 °C, the as-obtained samples were denoted as S-500, S-600, and S-700, respectively.

Structural Characterization. Structure, elemental and chemical states, morphology, automated area, and pore size properties of the samples were characterized by using a Bruker D8 Advanced X-ray diffractometer (Cu Kα radiation), XPS (X-ray photoelectron spectroscopy), transmission electron microscope (Tecnai G2 F30 S-TWIN), field-emission scanning electron microscope (Hitachi-S4800), RenishawInVia, automated area and pore size analyzer (Micrometrics ASAP 2010). Electromagnetic parameters with 10 wt % of paraffin were measured by using a Agilent PNA N5244A vector network analyzer.

RESULTS AND DISCUSSION

The formation process of 3DPCNs is schematically presented in Figure 1a. First, the glucose as a carbon precursor self-assembled on the multiple-scaled salts Na_2CO_3 by a freeze-drying method. Then the 3DPCN was obtained after glucose carbonization. In this phase, multiscales from nanometer to micrometer were achieved during salt crystallization. The as-prepared 3DPCNs were further purified by removing salts in distilled water. The synthesis process of ZnO@NPC/3DPCN is illustrated in Figure 1b. The Zn^{2+} precursor of ZIF-8 formed mixture first with 3DPCNs in methanol. Then, methanol solution mixed with 2-MeIm was poured into the solution of the ZIF-8 nucleus precursor. To further grow ZnO@NPC in 3DPCNs, ZIF-8 particles were first germinated in 3DPCNs, where 3DPCNs act as the substrate to load ZIF-8 forming ZIF-8/3DPCN composites. Then the ZnO@NPC/3DPCN hybrids were obtained after calcining the ZIF-8/3DPCN composites.

With salt templates synthesized, the morphology of 3DPCNs are shown in Figures 1c and S2d. It has interconnected porous networks with macropores (≥500 nm). In addition, desorption and nitrogen adsorption isotherms of ZnO@NPC/3DPCN were conducted to further inspect the structural features (Figure S1). The isotherm curves of S-600 indicate the coexistence of micropores and mesopores. This construction forms a large electron conducting network, which significantly promotes the transportation of electrons, enhances microwave energy attenuation and leads to boosting wastage of the microwave (Figure 1d).[26] ZIF-8/3DPCN composite SEM image is presented in Figure S2a, which indicates the successful synthesis of ZIF-8 on 3D carbon networks. The SEM image of S-600 (Figure 1d) shows ZnO@NPC polyhedrons uniformly grown into the interconnected networks. The SEM images of S-500 and S-700 are also shown in Figure S2b,c. With the increase of calcination temperatures, the particles size become smaller and the carbon network tends to collapse. Likewise, the TEM image in Figure 1e suggests that the ZnO@NPC particles integrated well with the 3DPCNs. The lattice spacing of ZnO (0.218 nm), the inset in the HRTEM image (Figure 1f) shows the existence of embedded ZnO@NPC particles.

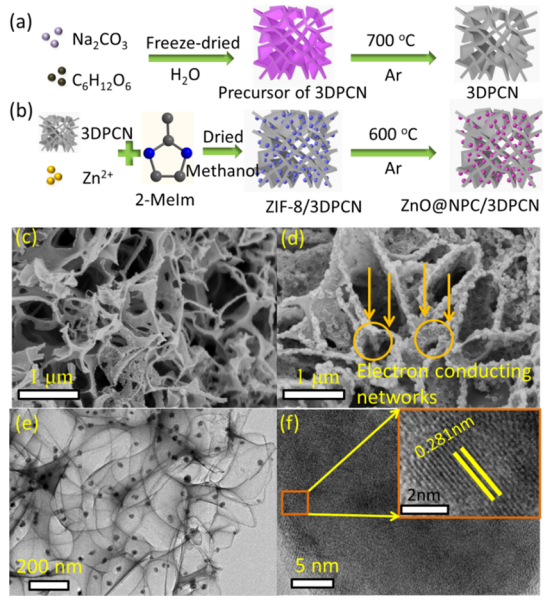

Figure 1. Composite diagrams of 3DPCNs (a) and ZnO@NPC/3DPCN hybrids (b); SEM images of 3DPCNs (c) and S-600 (d); TEM image (e) and HRTEM image (f) of S-600.

The XRD pattern of ZIF-8/3DPCN composites is shown in Figure S3, in which the diffraction peaks are corresponding to the XRD patterns of ZIF-8.[6] There are no obvious peaks of carbon due to the strong peaks of ZIF-8. However, from Figure 2a, one can find that the XRD patterns of S-500, S-600, and S-700 are very similar. A typical XRD pattern with a broad peak appears at 22°, which is assigned to the carbon network sheets. The small peaks appearing at 47.5° demonstrate the existence of ZnO,[6] which indicated that the ZnO concentrated on the nanopores has poor crystallization. The XPS spectra of S-600 hybrids are shown in Figure 2b. From Figure 2c, two typical peaks located at 1022.4 and 1045.5 eV are defined as Zn $2p_{3/2}$ and Zn $2p_{1/2}$. Meanwhile, two peaks located at 532.38 and 531.21 eV in the O 1s spectrum, shown in Figure 2d, can be likely defined as the chemisorbed oxygen and the lattice O of ZnO.[6] This phenomenon also proves the existence of zinc oxide. The C 1s spectra (Figure 2e) were grouped into three fitting peaks, according to C═O arising at 286.9 eV, C−O

DOI: 10.1021/acsami.9b08365
ACS Appl. Mater. Interfaces 2019, 11, 30228−30233

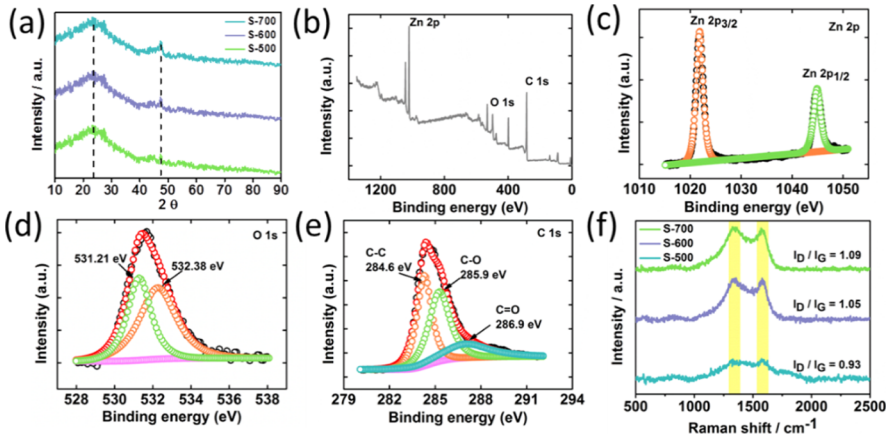

Figure 2. (a) XRD pattern of S-500/600/700; (b) wide XPS spectra of S-600; (c) Zn 2p, (d) O 1s, (e) C 1s XPS spectra of S-600 and (f) Raman spectra of S-500/600/700.

appearing at 285.9 eV and C−C emerging at 284.6 eV.[27] Furthermore, Raman spectra of S-500/600/700 are shown in Figure 2f, exhibiting a G band at 1580 cm^{-1} and a D band at 1346 cm^{-1}. The intensity ratio of D/G (I_D/I_G) are S-700 > S-600 > S-500, indicating the high density of topological vacancies and defects with the increasing of heating treatment temperatures.

The relationship between microwave absorption performance and ZnO@NPC/3DPCN hybrids were studied intrinsically. Many tests were conducted to analyze hierarchically from microwave response to microwave energy conversion of ZnO@NPC/3DPCN hybrids. Microwave energy conversion of ZnO@NPC/3DPCN composites is demonstrated in Figure 3a. In the carbon layers, abundant defects and functional

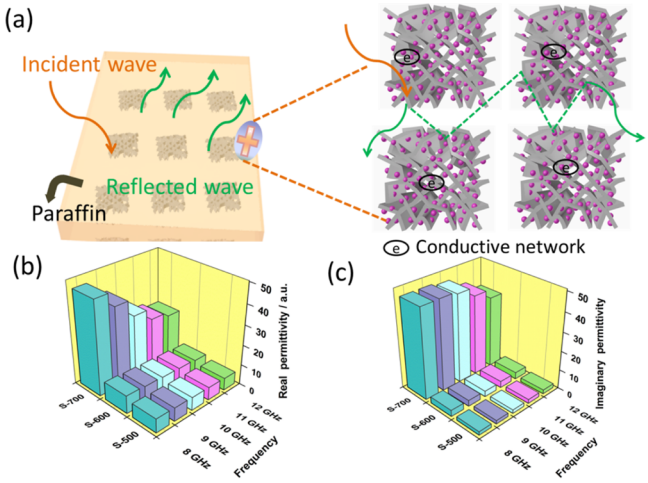

Figure 3. (a) Illustration of microwave attenuation hierarchically dissecting from microwave incidence to organization structure; (b) ε' and (c) ε'' of all samples.

groups induced the formation of dipoles.[28] Because of relaxation loss, the dipoles will promote microwave energy converted to electron kinetic energy. In Figure 3a, 3DPCNs established tight building conductive networks where electrons could absorb and consume microwave energy by migrating in networks.[28] Electrons need to assimilate more microwave energy to jump over carbon network layers.[29] Polarization is enhanced because of conduction loss and variable range hopping related to the charge transport behavior.[30] Moreover, network conductivity improved, which converted more microwave energy to electron kinetic energy. Besides, ZnO@NPC/3DPCN hybrids show disparate reflection manifestations, which was due to diverse impedance matching affected by charge transport on the ZnO@NPC and 3DPCN surface.

Figure S4a,b demonstrated that storage (ε') and wastage (ε'') ability of microwave could be well tuned by adjusting different heating treatment temperature in the whole 2−18 GHz. The complex permittivity ($\varepsilon_r = \varepsilon' - j\varepsilon''$) of diverse hybrids conducted in X-band frequency range are presented in Figure 3b,c. S-700 shows higher real and imaginary permittivity in X-band, indicating high contribution to dielectric loss. The permittivity of S-500, S-600, and S-700 hybrids increase significantly with the increased temperature. Hence, adjusting heating treatment temperature could be an efficient method to regulate dielectric properties of composites. As is known to all, conductivity determines dielectric properties of the composites. In addition, Figure S4c presents the electrical conductivity calculated from the equation $\sigma = \varepsilon_0\varepsilon''2\Pi f$, which illustrates a strong relationship between ε'' and conductivity. Conductivity represents the conduction loss. High conductivity could lead to high conduction loss. With the increased heating temperature, the conductivity of the hybrids has also increased that is also consistent with the results of Figure S4b. The tangent loss, tan δ (tan $\delta_\varepsilon = \varepsilon''/\varepsilon'$),[31] offers a measure of microwave energy lost in contrast to total microwave energy storage. As the temperature increased, the highest tangent loss of ZnO@NPC/3DPCN composites revealed a remarkable increase from 0.32 (S-500) to 0.53 (S-600) and then to 0.81 (S-700) (Figure S5), indicating improved microwave attenuation ability. Nevertheless, for microwave absorbing, tangent loss, attenuation α, and impedance matching are equally vital to generate a large reflection loss from the abovementioned. The attenuation ability standing for integral losses capability is evaluated by α ($\alpha = 2^{1/2}\Pi f((\mu''\varepsilon'' - \mu'\varepsilon') + ((\mu''\varepsilon'' - \mu'\varepsilon')^2 + (\mu'\varepsilon'' + \mu''\varepsilon')^2)^{1/2})^{1/2}/c$).[32] The overall trend of attenuation constant is S-700 > S-600 > S-500 (Figure 4a) in all frequency ranges. The impedance matching ($Z = |Z_{in}/Z_0|$) could determine the transmission performance of microwaves. More microwaves could access absorbers and be dissipate if the impedance matching is well, otherwise the microwaves could be reflected at the front surface of the absorbers. Fewer microwave reflection takes place on the absorber surface when the value

DOI: 10.1021/acsami.9b08365
ACS Appl. Mater. Interfaces 2019, 11, 30228−30233

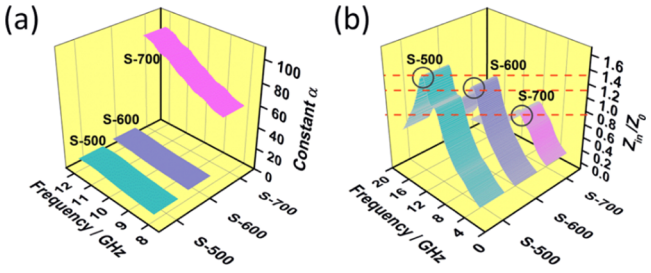

Figure 4. 3D maps for frequency dependence of the attenuation constant α (a) and impedance matching ratio (b) of all the hybrids.

of Z approaches 1. As shown in Figure 4b, inferior impedance matchings are assigned to the larger or smaller Z originated from higher or lower temperature. On the contrary, S-600 presents greatest impedance matching performance and moderate attenuation capability due to its relatively low complex permittivity. Consequently, S-600 exhibits excellent microwave absorption performance with moderate attenuation ability and best impedance matching.

An outstanding absorber should consider both impedance matching and RL at the same time instead of single performance. On the basis of a generalized transmission line theory[32] and the model of metal back plane, the RL values of microwave absorption composites could be calculated. The minimum RL values of S-600 hybrids in 2−18 GHz is −34.7 dB (Figure 5b), which is much better than S-500 (Figure 5a) and S-700 (Figure 5c). To further study the relationship of frequency and thicknesses, RL values of all composites with different thicknesses are also calculated (Figure 5d−f) in the X-band. Distinctly, S-700 exhibits a poor RL behavior lower than

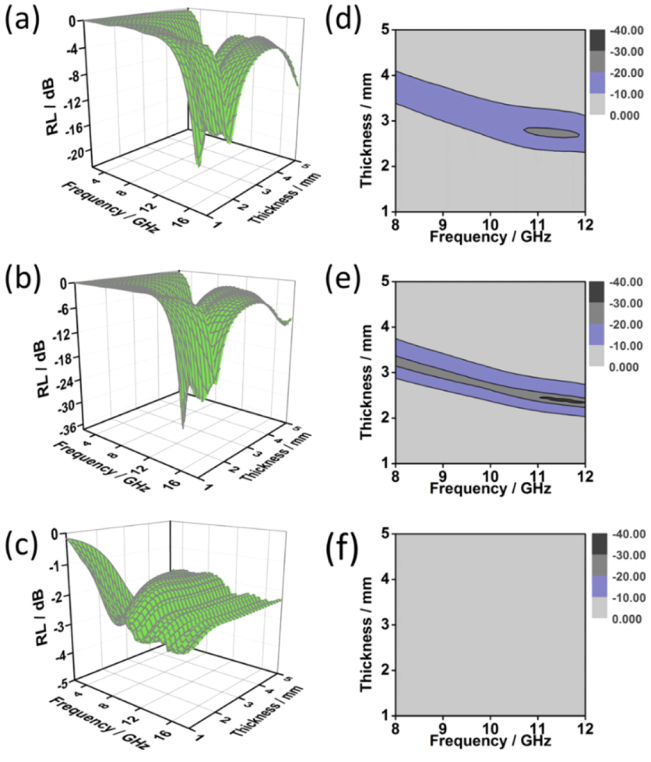

Figure 5. 3D images of calculating reflection loss values of hybrids for (a) S-500, (b) S-600, and (c) S-700 in full range of frequency; RL values of the (d) S-500, (e) S-600, and (f) S-700 hybrids with different thicknesses in the X-band.

−10 dB at the X-band with a thickness of 1−5 mm, which presents inferior microwave absorption properties. On the contrary, S-500 and S-600 show good microwave absorption performance in X-band, in which the S-600 has a better RL at lower thicknesses and lower filler loading ratios. The RL and filler loading ratio compared with the previous studies have been shown in Table S1. The results indicate that the synthesized ZnO@NPC/3DPCN hybrids in this work have better microwave absorption properties with lower filler loading ratios. These results illustrate the excellent characteristics of S-600 hybrids and their outstanding merits as microwave candidates.

To illustrate the influence of ZnO contents on microwave absorption, the contents of ZnO were controlled by different addition of Zn^{2+}, which were displayed in TG curves (Figure S6). There is a slight mass loss below 200 °C, which is due to the evaporation of adsorbed water. A second mass loss between 430 and 580 °C is concerned with the oxidation of carbon in the ZnO@NPC/3DPCN hybrids. There is no significant mass loss after 580 °C, indicating that carbon has completely burned out, only leaving the ZnO residue. The different contents of ZnO in ZnO@NPC/3DPCN composites are 18.25 and 35.76 wt %, respectively, which is corresponding to the addition of Zn^{2+}. The permittivity and RL with 2.2 mmol addition of Zn^{2+} have been shown in Figure S7. Compared with the addition of 1.1 mmol Zn^{2+} (Figure S4) composites, the real and imaginary parts of permittivity of 2.2 mmol additions were all decreased (Figure S7a), which led to poor impedance matching. The microwave absorption properties of 2.2 mmol addition Zn^{2+} is presented in Figure S7b. The maximum RL value is −13.2 dB with 2.35 mm matching thickness, which is inferior to the Zn^{2+} addition of 1.1 mmol. To further illustrate the outstanding microwave absorption performance of ZnO@NPC/3DPCN hybrids, the comparison of ZnO@NPC/3DPCN and ZnO/3DPCN is shown in Figure S8. Compared with the ZnO@NPC/3DPCN, the ZnO/3DPCN reveals poor RL of −19.1 dB with 2.35 mm, which also indicates that ZnO@NPC/3DPCN has excellent wave absorbing properties.

In addition, 3D RL curves of all composites at three diverse thicknesses in the X-band are presented in Figure 6a−c. For S-500, the RL didn't reach −20 dB with the frequency aggrandizing. And the RL value of S-700 is lower than −5 dB even at high frequency. Surprisingly, S-600 in Figure 6a exhibits a maximum RL of −35.7 dB with a corresponding thickness of 2.35 mm, and it exhibits the best frequency efficient bandwidth (Figure 6d) with 2.75 GHz in the livelong X-band with a thickness of 2.55 mm. Considering the traits of a wide bandwidth, small thickness, and strong absorption, the S-600 could act as an ideal absorbing composite.

Relevant mechanisms for improved microwave absorption performance are shown in Figure 7. Two main factors are summarized below:

Dipole Polarization. The dipole polarization can greatly influence the dielectric loss. A deeper study about polarization mechanisms is obtained via cole−cole curves in Figures 7 and S9. A semicircle represents a dielectric relaxation process. Distinctly, S-600 (Figure 7) possesses more semicircles than other composites (Figure S9), which leads to dielectric polarizations from 3DPCN arrays, ZnO particles and nanoporous carbon. All of them are contributed to improve microwave absorption on account of dipole polarization.

DOI: 10.1021/acsami.9b08365
ACS Appl. Mater. Interfaces 2019, 11, 30228−30233

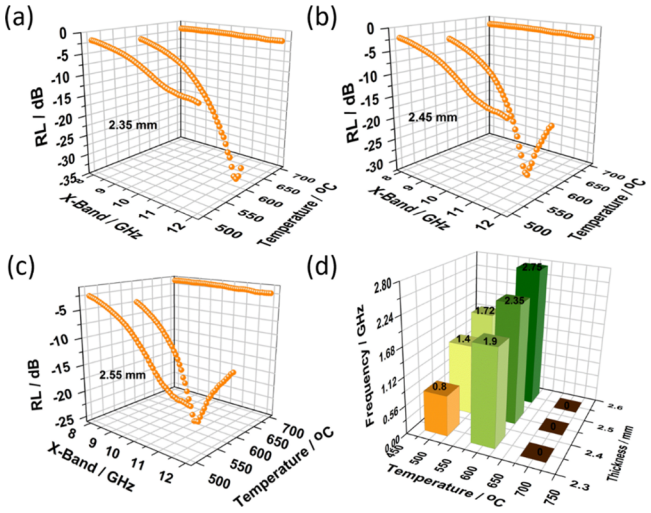

Figure 6. 3D plots RL of all hybrids vs frequency at diverse thicknesses (a–c); 3D image of the efficient frequency bandwidth for all the samples (d).

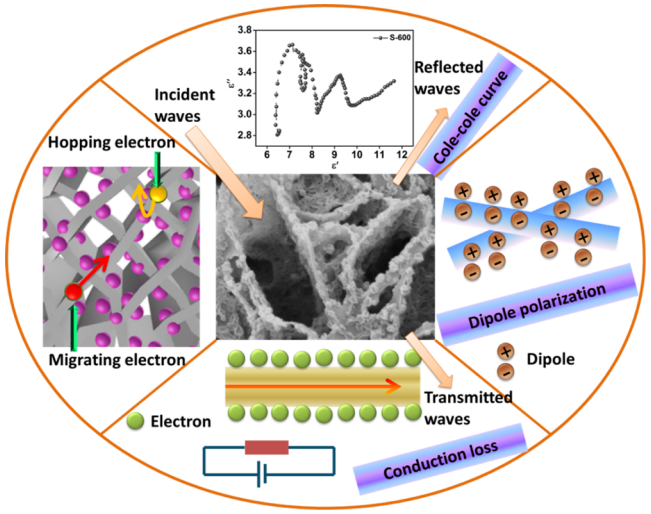

Figure 7. Schematic mechanisms of microwave absorption properties for ZnO@NPC/3DPCN hybrids.

Conduction Loss. The 3DPCN porous structures could allow more microwaves to be attenuated. Furthermore, the interfaces between ZnO and carbon materials increase the dielectric loss. In addition, the conductive network induced by the carbon network will help migrating electrons and hopping electron transfer easily, which leads to more microwave energy converted into electron kinetic energy. Therefore, microwave attenuation effect is achieved.

CONCLUSIONS

In conclusion, a nanocage network porous structure was synthesized via freeze-drying and in situ integrated ZIF-8 into 3DPCNs. Then the ZIF-8/3DPCN was derived into ZnO@NPC/3DPCN hybrids with direct carbonization. Chief of all, 3D carbon networks act as the nucleation sites for ZIF-8 granules, the microwave contact sites as well as the electron conducting pathways. Additionally, S-600 possesses more moderate electrical conductivity and excellent impedance matching, which is beneficial for microwave absorption. The maximum RL value reaches −35.7 dB with a 10 wt % filler loading. The facile synthesis of ZnO@NPC/3DPCN hybrids reveals multiple applications as light and strong microwave response. These carbon networks not only offer a strategy to produce pores inside carbon sheets but also propose a new idea for developing a better microwave absorber. In addition, the direct calcination method of MOF-carbons is promising for obtaining nanoporous carbon materials.

ASSOCIATED CONTENT

Supporting Information

The Supporting Information is available free of charge on the ACS Publications website at DOI: 10.1021/acsami.9b08365.

Nitrogen sorption isotherms, SEM and TEM images, permittivity, tangent dielectric loss, the cole−cole curves of the hybrids, RL, and filler loading ratios compared with the previous studies, TG curves, permittivity, and RL comparison (PDF)

AUTHOR INFORMATION

Corresponding Authors

*E-mail: gbji@nuaa.edu.cn. Phone: +86-25-52112902 (G.J.).
*E-mail: yuting@ntu.edu.sg. Phone: +65 63167899 (T.Y.).

ORCID

Guangbin Ji: 0000-0002-5150-3949
Ting Yu: 0000-0001-5782-1588

Author Contributions

The manuscript was written through contributions of all the authors. All the authors approved the final version of the manuscript.

Notes

The authors declare no competing financial interest.

ACKNOWLEDGMENTS

Financial supports from the National Nature Science Foundation of China (no. 11575085), the Aeronautics Science Foundation of China (no. 2017ZF52066), the Chinese Government Scholarship (no. 201806830052), the Postgraduate Research & Practice Innovation of Jiangsu Province (no. KYCX18_0277), the Qing Lan Project, Six talent peaks project in Jiangsu Province (no. XCL-035), the Open Research Fund of Jiangsu Provincial Key Laboratory for Nanotechnology of Nanjing University, the foundation of Jiangsu Provincial Key Laboratory of Bionic Functional Materials, and the Priority Academic Program Development of Jiangsu Higher Education Institutions (PAPD) are gratefully acknowledged.

REFERENCES

(1) Chen, C.; Yu, D.; Zhao, G.; Du, B.; Tang, W.; Sun, L.; Sun, Y.; Besenbacher, F.; Yu, M. Three-Dimensional Scaffolding Framework of Porous Carbon Nanosheets Derived From Plant Wastes for High-Performance Supercapacitors. *Nano Energy* **2016**, *27*, 377−389.
(2) Wang, Z.-L.; Xu, D.; Wang, H.-G.; Wu, Z.; Zhang, X.-B. In Situ Fabrication of Porous Graphene Electrodes for High-Performance Energy Storage. *ACS Nano* **2013**, *7*, 2422−2430.
(3) Wang, F.; Jiao, H.; He, E.; Yang, S.; Chen, Y.; Zhao, M.; Song, X. Facile Synthesis of Ultrafine SnO_2 Nanoparticles Embedded in Carbon Networks as a High-Performance Anode for Lithium-Ion Batteries. *J. Power Sources* **2016**, *326*, 78−83.
(4) Song, W.-L.; Cao, M.-S.; Fan, L.-Z.; Lu, M.-M.; Li, Y.; Wang, C.-Y.; Ju, H.-F. Highly Ordered Porous Carbon/Wax Composites for Effective Electromagnetic Attenuation and Shielding. *Carbon* **2014**, *77*, 130−142.

DOI: 10.1021/acsami.9b08365
ACS Appl. Mater. Interfaces 2019, 11, 30228−30233

(5) Liu, W.; Li, H.; Zeng, Q.; Duan, H.; Guo, Y.; Liu, X.; Sun, C.; Liu, H. Fabrication of Ultralight Three-Dimensional Graphene Networks with Strong Electromagnetic Wave Absorption Properties. *J. Mater. Chem. A* **2015**, *3*, 3739−3747.
(6) Liang, X.; Quan, B.; Ji, G.; Liu, W.; Zhao, H.; Dai, S.; Lv, J.; Du, Y. Tunable Dielectric Performance Derived from the Metal-Organic Framework/Reduced Graphene Oxide Hybrid with Broadband Absorption. *ACS Sustainable Chem. Eng.* **2017**, *5*, 10570−10579.
(7) Petit, C.; Bandosz, T. J. Synthesis, Characterization, and Ammonia Adsorption Properties of Mesoporous Metal-Organic Framework (MIL(Fe))-Graphite Oxide Composites: Exploring the Limits of Materials Fabrication. *Adv. Funct. Mater.* **2011**, *21*, 2108−2117.
(8) Furukawa, H.; Cordova, K. E.; O'Keeffe, M.; Yaghi, O. M. The Chemistry and Applications of Metal-Organic Frameworks. *Science* **2013**, *341*, 1230444.
(9) Liang, X.; Quan, B.; Sun, Y.; Ji, G.; Zhang, Y.; Ma, J.; Li, D.; Zhang, B.; Du, Y. Multiple Interfaces Structure Derived from Metal-Organic Frameworks for Excellent Electromagnetic Wave Absorption. *Part. Part. Syst. Charact.* **2017**, *34*, 1700006.
(10) Zhang, X.; Ji, G.; Liu, W.; Quan, B.; Liang, X.; Shang, C.; Cheng, Y.; Du, Y. Thermal Conversion of an Fe_3O_4@Metal-Organic Framework: A New Method for an Efficient Fe-Co/Nanoporous Carbon Microwave Absorbing Material. *Nanoscale* **2015**, *7*, 12932−12942.
(11) Liu, W.; Liu, J.; Yang, Z.; Ji, G. Extended Working Frequency of Ferrites by Synergistic Attenuation through a Controllable Carbothermal Route Based on Prussian Blue Shell. *ACS Appl. Mater. Interfaces* **2018**, *10*, 28887−28897.
(12) Quan, B.; Liang, X.; Zhang, X.; Xu, G.; Ji, G.; Du, Y. Functionalized Carbon Nanofibers Enabling Stable and Flexible Absorbers with Effective Microwave Response at Low Thickness. *ACS Appl. Mater. Interfaces* **2018**, *10*, 41535−41543.
(13) Tang, J.; Yamauchi, Y. MOF Morphologies in Control. *Nat. Chem.* **2016**, *8*, 638−639.
(14) Xu, H.; Yin, X.; Zhu, M.; Li, M.; Zhang, H.; Wei, H.; Zhang, L.; Cheng, L. Constructing Hollow Graphene Nano-Spheres Confined in Porous Amorphous Carbon Particles for Achieving Full X Band Microwave Absorption. *Carbon* **2019**, *142*, 346−353.
(15) Liu, Z.; Yuan, J.; Zhang, H.; Xiong, K.; Jin, S.; Wang, P. Enhanced Microwave Absorption Properties of Metal Organic Framework (MOF)-Derived Carbonaceous ZnO Incorporated Reduced Graphene Oxide Composites. *Nano* **2019**, *14*, 1950005.
(16) Jia, H.; Xing, H.; Ji, X.; Gao, S. Synergistic Effect of Hexagonal Flake Co_3O_4@PANI Core-Shell Composites with Excellent Microwave-Absorbing Properties. *J. Mater. Sci.: Mater. Electron.* **2019**, *30*, 3386−3395.
(17) Zhou, C.; Wu, C.; Liu, D.; Yan, M. Metal-Organic Framework Derived Hierarchical Co/C@V_2O_3 Hollow Spheres as a Thin, Lightweight, and High-Efficiency Electromagnetic Wave Absorber. *Chem.—Eur. J.* **2019**, *25*, 2234−2241.
(18) Wang, Y.; Zhang, W.; Wu, X.; Luo, C.; Wang, Q.; Li, J.; Hu, L. Conducting Polymer Coated Metal-Organic Framework Nanoparticles: Facile Synthesis and Enhanced Electromagnetic Absorption Properties. *Synth. Met.* **2017**, *228*, 18−24.
(19) Hsu, S.-H.; Li, C.-T.; Chien, H.-T.; Salunkhe, R. R.; Suzuki, N.; Yamauchi, Y.; Ho, K.-C.; Wu, K. C.-W. Platinum-Free Counter Electrode Comprised of Metal-Organic-Framework (MOF)-Derived Cobalt Sulfide Nanoparticles for Efficient Dye-Sensitized Solar Cells (DSSCs). *Sci. Rep.* **2014**, *4*, 6983.
(20) Torad, N. L.; Li, Y.; Ishihara, S.; Ariga, K.; Kamachi, Y.; Lian, H.-Y.; Hamoudi, H.; Sakka, Y.; Chaikittisilp, W.; Wu, K. C.-W.; Yamauchi, Y. MOF-Derived Nanoporous Carbon as Intracellular Drug Delivery Carriers. *Chem. Lett.* **2014**, *43*, 717−719.
(21) Salunkhe, R. R.; Young, C.; Tang, J.; Takei, T.; Ide, Y.; Kobayashi, N.; Yamauchi, Y. A High-Performance Supercapacitor Cell Based on ZIF-8-Derived Nanoporous Carbon Using an Organic Electrolyte. *Chem. Commun.* **2016**, *52*, 4764−4767.
(22) Zhang, W.; Jiang, X.; Zhao, Y.; Carné-Sánchez, A.; Malgras, V.; Kim, J.; Kim, J. H.; Wang, S.; Liu, J.; Jiang, J.-S.; Yamauchi, Y.; Hu, M. Hollow Carbon Nanobubbles: Monocrystalline MOF Nanobubbles and Their Pyrolysis. *Chem. Sci.* **2017**, *8*, 3538−3546.
(23) Young, C.; Wang, J.; Kim, J.; Sugahara, Y.; Henzie, J.; Yamauchi, Y. Controlled Chemical Vapor Deposition for Synthesis of Nanowire Arrays of Metal-Organic Frameworks and Their Thermal Conversion to Carbon/Metal Oxide Hybrid Materials. *Chem. Mater.* **2018**, *30*, 3379−3386.
(24) Wang, C.; Kaneti, Y. V.; Bando, Y.; Lin, J.; Liu, C.; Li, J.; Yamauchi, Y. Metal-Organic Framework-Derived One Dimensional Porous or Hollow Carbon-Based Nanofibers for Energy Storage and Conversion. *Mater. Horiz.* **2018**, *5*, 394−407.
(25) Zhu, S.; Li, J.; He, C.; Zhao, N.; Liu, E.; Shi, C.; Zhang, M. Soluble Salt Self-Assembly-Assisted Synthesis of Three-Dimensional Hierarchical Porous Carbon Networks for Supercapacitors. *J. Mater. Chem. A* **2015**, *3*, 22266−22273.
(26) Deng, X.; Zhu, S.; Li, J.; Ma, L.; He, F.; Liu, E.; He, C.; Shi, C.; Li, Q.; Zhao, N. Ball-in-Cage Nanocomposites of Metal-Organic Frameworks and Three-Dimensional Carbon Network: Synthesis and Capacitive Performance. *Nanoscale* **2017**, *9*, 6478−6485.
(27) Man, Z.; Li, P.; Zhou, D.; Zang, R.; Wang, S.; Li, P.; Liu, S.; Li, X.; Wu, Y.; Liang, X.; Wang, G. High-Performance Lithium-Organic Batteries by Achieving 16 Lithium Storage in Poly(Imine-Anthraquinone). *J. Mater. Chem. A* **2019**, *7*, 2368−2375.
(28) Cao, M.; Wang, X.; Cao, W.; Fang, X.; Wen, B.; Yuan, J. Thermally Driven Transport and Relaxation Switching Self-Powered Electromagnetic Energy Conversion. *Small* **2018**, *14*, 1800987.
(29) Cao, M.-S.; Song, W.-L.; Hou, Z.-L.; Wen, B.; Yuan, J. The Effects of Temperature and Frequency on the Dielectric Properties, Electromagnetic Interference Shielding and Microwave-Absorption of Short Carbon Fiber/Silica Composites. *Carbon* **2010**, *48*, 788−796.
(30) Quan, B.; Liang, X.; Ji, G.; Ma, J.; Ouyang, P.; Gong, H.; Xu, G.; Du, Y. Strong Electromagnetic Wave Response Derived from the Construction of Dielectric/Magnetic Media Heterostructure and Multiple Interfaces. *ACS Appl. Mater. Interfaces* **2017**, *9*, 9964−9974.
(31) Quan, B.; Liang, X.; Xu, G.; Cheng, Y.; Zhang, Y.; Liu, W.; Ji, G.; Du, Y. A Permittivity Regulating Strategy to Achieve High-Performance Electromagnetic Wave Absorbers with Compatibility of Impedance Matching and Energy Conservation. *New J. Chem.* **2017**, *41*, 1259−1266.
(32) Liang, X.; Quan, B.; Chen, J.; Gu, W.; Zhang, B.; Ji, G. Nano Bimetallic@Carbon Layer on Porous Carbon Nanofibers with Multiple Interfaces for Microwave Absorption Applications. *ACS Appl. Nano Mater.* **2018**, *1*, 5712−5721.

DOI: 10.1021/acsami.9b08365
ACS Appl. Mater. Interfaces 2019, 11, 30228−30233